Title: Drone-assisted collection of environmental DNA from tree branches for biodiversity monitoring

Authors:
Emanuele Aucone[1,2,], Steffen Kirchgeorg[1,2], Alice Valentini[3], Loïc Pellissier[2,4], Kristy Deiner[5], Stefano Mintchev[1,2*]

Affiliations:
[1]Environmental Robotics Laboratory, Department of Environmental Systems Science, Swiss Federal Institute of Technology (ETH) Zürich: Zürich, Switzerland.
[2]Swiss Federal Institute for Forest, Snow and Landscape Research WSL: Birmensdorf, Switzerland.
[3]SPYGEN: Le Bourget du Lac, France.
[4]Ecosystems and Landscape Evolution Group, Department of Environmental Systems Science, Swiss Federal Institute of Technology (ETH) Zürich: Zürich, Switzerland.
[5]Environmental DNA Group, Department of Environmental Systems Science, Swiss Federal Institute of Technology (ETH) Zürich: Zürich, Switzerland.
*Corresponding author. Email: stefano.mintchev@usys.ethz.ch

Abstract: The protection and restoration of the biosphere is crucial for human resilience and well-being, but the scarcity of data on the status and distribution of biodiversity puts these efforts at risk. DNA released into the environment by organisms, i.e., environmental DNA (eDNA), can be used to monitor biodiversity in a scalable manner if equipped with the appropriate tool. However, the collection of eDNA in terrestrial environments remains a challenge due the many potential surfaces and sources that need to be surveyed and their limited accessibility. Here, we propose to survey biodiversity by sampling eDNA on the outer branches of tree canopies with an aerial robot. The drone combines a force-sensing cage with a haptic-based control strategy to establish and maintain contact with the upper surface of the branches. Surface eDNA is then collected using an adhesive surface integrated in the cage of the drone. We show that the drone can autonomously land on a variety of branches with stiffness between 1 and 10^3 Newton/meter, without prior knowledge of their structural stiffness, and with robustness to linear and angular misalignments. Validation in the natural environment demonstrates that our method is successful in detecting animal species, including arthropods and vertebrates. Combining robotics with eDNA sampling from a variety of unreachable above ground substrates can offer a solution for broad scale monitoring of biodiversity.

One-Sentence Summary:

A drone incorporating a force-sensing cage with adhesive surfaces enables environmental DNA to be collected from tree branches.

This document is the accepted manuscript version of the following article:
Aucone, E., Kirchgeorg, S., Valentini, A., Pellissier, L., Deiner, K., & Mintchev, S. (2023). Drone-assisted collection of environmental DNA from tree branches for biodiversity monitoring. Science Robotics, 8(74), eadd5762 (13 pp.).
https://doi.org/10.1126/scirobotics.add5762

Main Text:

INTRODUCTION

Biodiversity is declining rapidly, with an estimated one million species threatened with extinction in the next two decades (*1*), a loss of life on this scale will substantially alter the structure and functioning of whole ecosystems (*2–4*). Preserving the biosphere is therefore critical and urgent to meet the 2030 Agenda for Sustainable Development with its 17 Sustainable Development Goals (SDGs) (*5*, *6*). Protecting and restoring biodiversity depends on obtaining precise data on species distributions and population sizes on relevant ecological scales (*7–9*), which is currently limited by the lack of methods to scale data collection (*10*, *11*). Environmental DNA (eDNA) surveys have recently gained worldwide interest for biodiversity monitoring (*12–17*). Environmental DNA is the genetic material obtained directly from environmental samples (soil, sediment, water, air, etc.), and it is characterized by a complex mixture of intracellular (from living cells) or extracellular DNA (originating from shed skin, hairs, urine, feces, or carcasses) (*18*). Environmental DNA metabarcoding surveys can simultaneously detect multiple species from all three domains of life (Archaea, Bacteria and Eukarya) from a single sample without any obvious sign of their presence (*19*), and automated, mechanized methods to collect DNA traces have the potential to facilitate the survey of biodiversity over large spatial scales (*20*).

Aerial robots equipped with cameras or high-frequency trackers have successfully supported monitoring wildlife (*21–24*), and their versatility can also be adapted to collect eDNA samples. With the development of increasingly fast, sensitive, and inexpensive eDNA methods (*13*), the manual collection of relevant environmental samples remains a major bottleneck in scaling eDNA surveys. The manual labor involved and the complexities of reaching harsh and dangerous landscapes hinder eDNA surveys especially in terrestrial ecosystems. For example, plant structures (e.g., leaves, flowers, twigs, bark) have been swabbed to collect eDNA for detecting herbivores and arthropods (*25–27*). But even a seemingly simple task like swabbing a surface becomes difficult if not impossible in forest canopies, which are accessible only to trained climbers or through expensive infrastructures (*28*). The forest canopy represents an important habitat for biodiversity, which remains generally under surveyed (*29*). The use of robots to survey eDNA from such locations would allow us to improve the variety of habitats that can be monitored. Although robots have been successfully used to collect eDNA samples in water (*20*, *30–32*), surveying eDNA with drones in forests presents open scientific challenges in both robotics and biology.

The requirement of touching branches to collect eDNA translates into the need for the drone to establish contact with the surroundings by applying forces on surfaces. Aerial physical interaction requires a combination of hardware (e.g., omnidirectional vehicles, protective structures, robotic arms, and end-effectors) (*33*), direct (*34*, *35*) or indirect (*36*, *37*) force sensing, and control strategies including the most popular impedance and admittance control (*38–40*). Interaction tasks, such as perching (*41*, *42*), collision handling (*43*, *44*), contact-based inspection (*45–47*), and aerial manipulation (*48*, *49*) are typically limited to structures with rigid surfaces. However, branches are a non-static substrate whose compliance can vary by up to four orders of magnitude (*50*). For current physical interaction methods, the unknown elastic response of the branches, as well as misalignments during approach caused by unpredictable branch oscillations, can make the drone lose stability, tip over, or be hurled away. Similar challenges are encountered by animals, whose response to substrate compliance varies substantially among species. Although some arboreal specialists have developed biomechanical and behavioral adaptations to take advantage of elastic recoil from perches to jump and swing (*51–53*), for some birds, the difficulty in estimating the flexibility of branches causes notable stability problems on landing, requiring rapid corrections by the wings and tails to maintain balance (*54*). Moreover, the robots should be able

to collect eDNA, e.g., from the surface, but this has not been extensively tested on tree surfaces (*27*).

Here, we present a haptic-based control strategy for autonomously landing, establishing, and maintaining contact with branches with stiffness between 1 and 10^3 N/m. Our approach exploits a force-sensorized cage, to measure the interaction force between the drone and the branch and a high-level haptic-based controller that replans waypoints based on force measures to land on the branch. The eDrone uses this interaction strategy to establish and maintain contact on the upper surfaces of branches where eDNA is collected by a sticky surface integrated in the cage (Movie 1). The eDNA samples are then extracted and sequenced to identify the organisms to which the eDNA belongs (Fig. 1).

The work presented in this article makes three contributions to the field of robotics and biodiversity monitoring. First, we present the concept of a drone developed to physically interact with compliant branches. The eDrone is designed to maximize robustness to misalignments while landing on branches by being able to sense and handle single-point contacts from various directions and over a large body surface area. This is achieved by integrating the drone into a hemispherical end-effector with distributed force perception that also doubles as landing gear and protective cage. Second, we propose a high-level control strategy that infers force information for safe physical interaction with branches spanning four orders of magnitude of flexibility. The haptic-based landing strategy is reliable independent~~ly~~ of the location of the contact on the cage and of the stiffness of the environment. Furthermore, it does not require any prior knowledge of structural stiffness and geometry of the environment, nor a re-tuning if such parameters change. The physical interaction strategy is derived from a numerical model and experimentally validated with landings on mock and real branches. Last, we demonstrate that it is possible to successfully collect eDNA from a variety of animals in contact with the tree using sticky material integrated with the drone. During the outdoor landings, eDNA was successfully collected from the bark of 7 different trees, enabling the identification of 21 taxa, including insects, mammals, and birds.

RESULTS

The eDrone demonstrates the potential of exploiting robots for biodiversity monitoring by successfully sampling eDNA from tree branches (Fig. 1 and Movie 1). The drone is teleoperated over a branch of interest using visual feedback from an onboard camera. When the desired alignment is roughly achieved, the drone autonomously lands and rests on the branch (Fig. 1A). During this time, the eDNA collector on the outermost surface of the cage touches the bark to retrieve surface eDNA. The eDrone then returns to hover above the branch and is teleoperated back to a designated landing area where the eDNA collectors are removed and stored. The samples are then processed following the workflow of eDNA metabarcoding for a biodiversity survey (Fig. 1B). Field experiments resulted in the identification of 21 taxa among the *Metazoa* kingdom, spanning different animal classes like *Insecta*, *Mammalia*, *Aves*, *Collembola*, and *Amphibia* (Fig. 1C) from 7 distinct tree species.

Robot design rationale

The eDrone (Fig. 2A) consists of a quadcopter equipped with a force-sensing cage that incorporates eDNA collectors to retrieve surface eDNA from tree branches. The compliant nature of this substrate leads to challenges in the design of the branch-touching end-effector, the force sensing strategy and the eDNA collection mechanism based on surface touch.

Drones interacting with rigid structures~~,~~ favour a single-point end-effector to localize the interaction force in a targeted region and along a preferred direction. Whereas landing on flexible, non-static branches requires robustness to linear and angular misalignments that inevitably arise

from unpredictable movements of the branches. For this reason, we maximized the interaction surfaces by integrating a hemispherical cage under the quadcopter's frame instead of a single point end-effector. The cage consists of four vertical arcs connected to a horizontal ring (Fig. 2A). The drone can touch branches along each arc, enabling multidirectional interactions and robustness to linear misalignments (Fig. 2C). The diameter of the cage is the result of a trade-off between conflicting requirements. On the one hand, a large cage tolerates larger misalignments and distances the drone further from vegetation, reducing the risks of twigs or leaves getting caught in the propellers. On the other hand, a cage with a small footprint makes the drone more suitable for flying in cluttered environments and reduces the destabilizing moment caused by the interaction force with the branch (see Fig. S2). Thus, the eDrone has a cage with the minimum diameter needed to enclose the four propellers, and tolerates misalignments up to 220 mm per side. We also added a circular fiberglass strip around the ring to further shield the propellers from the vegetation. A high-friction material is bonded to the outer surface of the arcs to minimize slippage (Fig. 2B); the addition of cantilevers (placed at 25°, 50°, and 75° on each arc of the hemisphere, Fig. 2C) allows the drone to cling to the branch if frictional adhesion fails.

The force sensing strategy relies on a six-axis load cell, which connects the caged end-effector to the frame of the aerial robot (Fig. 2A). Despite being centralized, this haptic-sensing system offers a distributed perception awareness by measuring the interaction force at the contact point, which can occur anywhere along the four arcs of the cage. Each arc of the cage contains an eDNA collection mechanism. They consist of thin fiberglass flaps whose outermost surface can be covered with an adhesive material (tape or humified gauze, see Material and Methods). During landing, the flap is pressed against the branch and genetic material is retrieved from the bark (Fig. 2B). The flexible flap partially wraps around the branch to increase the collection area (Tab. S1). The result of this design rationale is a 1.2-kg aerial robot with a circular footprint measuring 440 mm in diameter. Further details on the mechanical design and electronics for autonomous and teleoperated flight are available in Materials and Methods.

Landing strategy rationale

The eDrone lands and maintains contact with branches to collect eDNA. This interaction is made challenging because the stiffness (K) of the branches is unknown to the drone, and it can span between 10^3 N/m (rigid) and 1 N/m (compliant), as reported in (*50*). To develop the landing strategy, we studied the planar equilibrium of the eDrone on a beam with a flexural hinge. Whereas the complete model is presented in the Supplementary Materials, Fig. 3A reports the most relevant results. Given that the main objective of the landing is to maintain contact with the branch to collect eDNA, we explore how the drone can reduce the risk of slipping off the beam, i.e., how to minimize the ratio of the friction force (F_F) to the normal force (F_N). For stiff beams (i.e., K = 10^2 and 10^3 N/m), the risk of slipping is minimized by a near-vertical landing. However, when the beam becomes more compliant (i.e., K = 1 and 10 N/m) and the deflection of the beam increases (α), the drone needs to tilt (ϕ). Higher tilt angles are also needed as the drone applies increasing force on the beam (higher thrust reduction), and its deflection increases. We further evaluated the influence of non-zero initial inclination of the beam on landing. The model shows that tilting is needed even for stiff beams and increases for higher values of initial inclination and compliance (Fig. S3). Based on the analysis, we concluded that the drone can land on beams with inclination between ±20° with a safety margin to prevent the horizontal ring of the cage from colliding with the beam (Fig. S1). This condition must be avoided as the haptic-based control strategy is formalized for handling a single-point contact on the arcs of the cage.

These observations led to the rationalization of a three-phase landing strategy, in which the drone descends onto the branch, gradually leans on it, and then rests in equilibrium to collect eDNA (Fig. 3B and C). The strategy is implemented through a high-level controller, called the Haptic Waypoint Replanner (HWR), which executes the strategy as a state machine (Fig. 3D).

First, the drone is teleoperated above a branch and released in a hovering condition. Hence, it autonomously descends following a reference trajectory composed of vertical waypoints until the force-sensing cage detects a contract with the branch (Descending, Fig. 3B). We utilize a threshold on the vertical component of the force vector ($F_{z,min}$) to signal the contact. This threshold must be set higher than the noise of the load cell to avoid false contact detection during free-flight conditions (in our case, the threshold is set to 0.35 N).

Once the contact is detected, the HWR continues to command the drone to lean down via vertical waypoints (Leaning, Fig. 3B), reducing the thrust force and continuing to measure the interaction force (F_{ext} in Fig. 3C). During this phase, the HWR monitors potentially dangerous conditions, such as tipping or sliding off the branch, which would cause the drone to perform an evasive maneuver and get back to hovering. This, referred to as the "sliding condition" in the flow-chart (Fig. 3D), is accomplished by tracking the changes between the current position of the drone and its position during the first contact with the branch. The drone checks whether its position drifts more than a predefined maximum displacement value. If the drone does not slide, it continues to exert a higher force on the branch to secure the contact until a maximum vertical force is reached ($F_{z,max}$). As the collection of eDNA is not mediated by pressure, but rather by the transfer action of the collector material (see Section Proof-of-concept eDNA survey), we set this threshold as low as 1 N. This ensures that the drone remains within a safe operating range, as the branch does not bend too much and collisions with the horizontal ring of the cage are avoided (Fig. S1 and S3), and the risk of sliding is minimized for a low tilt angle (i.e., less than 5°, see Fig. 3A and S3). Moreover, the thrust is kept close to the hovering value, thus allowing for faster evasive maneuvers.

Once the threshold is reached, the drone transitions to the resting phase and maintains contact with the branch (Resting, Fig. 3B). This is obtained as the HWR commands a single 3D waypoint in the opposite direction of the resultant force. Indeed, starting from the current position, the 3D information of the external force is exploited as a position offset which is amplified by the controller gain (C_{gain} , Fig. 3C). If the branch is rigid, the resultant force is mainly vertical, and the waypoint is set along the vertical descent. However, if the branch is compliant, the lateral and longitudinal components of the force are not negligible, and the waypoint is offset from the vertical. This induces the drone to tilt and reduce the slipping risk as shown by the equilibrium model (Fig. 3A). We selected a C_{gain} that provides stable interaction for all stiffnesses in the range between 1 to 10^3 N/m. This was achieved by modeling the robot's dynamics during the resting phase and identifying boundary conditions for controller gain (see Supplementary Material). As a result, the landing strategy presents high-level problem abstraction and generality, combining no-prior knowledge of the environment with the versatility of a controller gain which does not need re-tuning if the environment changes.

Experimental validation of the HWR

An autonomous landing on a beam with stiffness K = 1 N/m is illustrated as an example in Fig. 4. When the drone starts leaning ($F_{z,min}$ overcome), its position in x and y drifts from the reference as the perch begins to bend vertically (zy plane) and laterally (zx plane), and the drone slightly slips (Fig. 4C). On the vertical axis, the drone starts loading down trying to track the z waypoint until the maximum threshold $F_{z,max}$ is reached (Fig. 4E) - in that moment there is a difference between the reference and the actual position of the drone (Fig. 4C). Thus, the resting phase engages, and the new waypoint is computed in the 3D space, not only vertically anymore, as it considers the longitudinal (F_x) and lateral (F_y) contributions of the force too. This causes the drone to tilt, as can be seen by the increase in the roll angle in Fig. 4D. As discussed above, tilting the drone on flexible perches reduces the risk of slipping. As expected, the final reference position (on all the axes) cannot be tracked with zero error as the waypoint is behind the structure. At this point, the

drone maintains contact with the beam as confirmed by Fig. 4E, which shows that the drone keeps the vertical force stable around $F_{z,max}$ (as it also keeps a stable z position, even without direct force control involved in the loop), while the oscillations on the lateral and longitudinal forces are kept small as the drone pushes in the direction of the resultant force vector.

We evaluated the robustness and versatility of the landing strategy through 110 landings on cantilever beams with different stiffnesses (1, 10, 10^2 and 10^3 N/m, see Movie S1 and Supplementary Materials). We performed the landings with an increasing level of linear misalignment corresponding to contact angles between the cage and the beam of 0° (Fig. 5A and B), 25°, 50°, and 75° (Fig. 5C and D). We assessed the stability of the drone by evaluating the amplitude of position oscillations around the mean value during the resting phase. For this purpose, we computed the standard deviation σ of the position error $\Delta p = \|p - \bar{p}\|_2 = \sqrt{(x-\bar{x})^2 + (y-\bar{y})^2 + (z-\bar{z})^2}$, where $p = [x, y, z]^T$ are the values of the position components over time and $\bar{p} = [\bar{x}, \bar{y}, \bar{z}]^T$ are the mean values.

Although the drone experiences higher amplitude oscillations when the compliance of the perch and the misalignment increases (Fig. 5A and C), the average amplitude is less than 15 mm with a peak of 40 mm for the most flexible perch and larger misalignment. The distributions of data acquired during the resting are statistically different from the "no-contact" hovering condition (significance of 99% for K = 10^3 N/m and 99.9% for K = 10^2, 10, 1 N/m). Furthermore, such distributions do not present any statistical difference when compared with each other, also in case of misalignment. This indicates that the stability of the interaction does not statistically differ even if the stiffness of the beam changes four orders of magnitude and if there is a large misalignment. We also report the average value of the interaction force magnitude during the resting phase (Fig. 5B and D). The hovering case in this graph is reported only to visualize the noise of the load cell during the "no-contact" condition. The results show that during the resting phase the drone constantly maintains contact by exerting an interaction force close to the maximum threshold independently of the flexibility of the perch and the misalignments. For stiff beams, as the structure does not substantially bend, the vertical component is the major contribution to the interaction force, hence the average value of the force is close to the vertical force threshold ($F_{z,max}$). For very flexible beams, instead, the bending of the structure results in lateral components of the interaction force, which cause an increase of the average force magnitude.

We then analyzed the robustness to angular misalignments, showing that the performances are guaranteed even if the contact occurs on the lateral arcs of the cage, instead of the frontal or rear one. We decided to compare the lateral axis case with the best case obtained on the frontal axis (contact at 50°) during the interaction with the most flexible perch (K = 1 N/m). The statistical analysis proves that the distributions of data are not statistically different, in terms of both position oscillations (Fig. 5E) and interaction force magnitude (Fig. 5F). Such a result confirms what we expected, as the overall strategy is general and exploits all the components of the force, thus it is symmetrical and independent of where the resultant interaction force occurs.

Finally, we validated the strategy in outdoor scenarios. Figure 6 reports the landing on the pine tree branch illustrated in Fig. 1A and Movie 1. The eDrone performs the landing procedures as planned, switching between the three states. As desirable, the amplitude of the oscillations stabilizes once the drone transitions to the resting phase and reaches a value comparable with that obtained in the indoor experiments (Fig. 5A and C). Similarly, the vertical component of the interaction force (F_z) remains stable around the maximum force threshold, ensuring that contact with the branch is maintained. The lateral and longitudinal components of the force show larger oscillations than in the indoor experiments. This could be a consequence of the oscillations induced by the wake of the propellers on the twigs underneath the drone (Movie 1).

Proof-of-concept eDNA survey

Once the eDrone is in contact with the branch, surface eDNA is collected by an adhesive surface attached to the flaps of the cage (Fig. 1A). We tested adhesive tape, and a cotton gauze humidified with a solution of water and DNA-free sugar (see Materials and Methods). We surveyed eDNA on 7 trees belonging to 5 different families: one *Cornus mas L.* (Cornaceae), three *Picea abis (L.) Karst.* (Pinaceae), one *Tilia cordata Mill.* (Malvaceae), one *Juglans nigra L.* (Juglandaceae), one *Forsythia x intermedia Zabel* (Oleaceae). We decided to select these different tree species, both angiosperms and gymnosperms, to test the efficacy of the landing strategy on branches with different morphology. For example, Pinaceae have branches with a regular cylindrical shape, similar to the beams used for indoor tests, while trees belonging to other taxa have more irregular branches with upward-pointing twigs that could hinder the drone's landing. Moreover, we selected Cornaceae and Oleaceae, which were in flower and showing considerable arthropod activity. The experiments were conducted in the Swiss lowlands in three consecutive days (16^{th}, 17^{th}, 18^{th} March 2022). We collected samples in the arboretum surrounding the Swiss Federal Institute for Forest, Snow and Landscape Research (WSL), where several tree species can be found and the vicinity to our research facility allows the most robust technical tests for the engineering aspects, e.g., access to battery charger and spare components. For safety reasons, the sampling points were chosen on isolated branches to avoid unwanted collision with vegetation during the approaching phase (Fig. 1A). We also favored branches with initial inclination close to zero, to remain within the safety inclination range of ±20° (Fig. S3).

Strips (approximately 240 mm long, 15 mm wide) of two different materials, adhesive tape and humidified gauze, were attached to the four flaps of the eDrone's cage. The eDrone performed a first landing, a 90° rotation around the yaw axis, and a second landing on each branch. In each landing, the resting phase lasted 10 seconds. The eDrone was then returned to the ground base, where the four strips were removed using sterile gloves and stored in a sterile 30 ml tube filled with 20-25 ml of CL1 buffer (SPYGEN, Le Bourget du Lac). We repeated the same procedure for both collector materials (tape and cotton gauze) on the same branch and used the visual feedback from the ground and from the drone camera to approach the same sampling point. Upon the 7 targeted trees, our field collection led to a total of 14 samples. Two negative controls, one for each type of collector material were also prepared by taking one of each collector type and placing them in the tubes without contact to tree surfaces. The 16 samples were analyzed using a metazoan universal primer to detect eDNA from animal species. The complete sterilization, collection and analysis protocols are reported in the Supplementary Materials.

We identified 21 taxa with a predominance of insects but also some vertebrates such as mammals, birds and amphibians. We observed a difference in detection of eDNA between sampling days (Fig. 7). Specifically, at the start of the experiment all the samples retrieved eDNA of animal species (i.e., both materials worked) including 10 arthropods and 5 vertebrates. In the last part of the experiments, we identified only a few species (including 7 new insects and 1 mammal), and the last day only the gauze presented DNA traces.

DISCUSSION

Sustainable development and climate protection must go hand in hand with the conservation of biodiversity in order to shape a livable future. The development of eDNA surveys is unlocking new possibilities for monitoring biodiversity–(*13*, *19*) and, in combination with drone-assisted eDNA collection, has the potential to be scaled up to verify the recovery and resilience of the biosphere.

The eDrone presented in this article offers a solution for the remote collection of eDNA from the upper surfaces of tree branches. To this end, we developed a strategy that enables a drone to

establish and maintain stable contact with flexible branches. This is achieved by combining a force-sensitive protective cage and a high-level controller based on force feedback. Starting from numerical and physical simulations, we proposed and validated a general methodology for landing on compliant branches with stiffness spanning four orders of magnitude, without prior knowledge of the environment and need for re-tuning. We have also demonstrated robustness to linear and angular misalignments.

The proof-of-concept eDNA survey gives us insight into future collaborative developments in robotics and the surveying of eDNA in terrestrial ecosystems. To offer more comprehensive surveys, more extensive tests under a variety of tree species or environmental conditions are required. In particular, on the last day of sampling we found a decline in detection associated with heavy rainfall the night before. Rainfall likely washed away the eDNA present on vegetation surfaces in agreement with recent findings on the fate of surface eDNA (*55*) and the use of artificial and natural rain-wash to collect eDNA from vegetation (*27*, *56*). This result suggests that the surface detection relates to recent animal activity, but the transport and fate of eDNA on above ground substrates should also be better understood to perform efficient survey. Moreover, the different performance of the two collectors suggests the need for in-depth investigations into the transfer of eDNA from different types of natural substrates under various environmental conditions, and the opportunity to use the results to develop optimized collector materials.

Beyond the present study, the system can be used to sample systematically a defined forest surface. Collecting a large number of samples per tree can enhance the estimation of a broader diversity of animals interacting with the tree surface, and a species-saturation analysis can provide an estimation of the sampling effort required to capture this diversity. However, this may lead to an increase sampling effort in the field and an increase eDNA analysis cost. One solution would be to pool the samples in the same collection tube before the eDNA extraction, to reduce the cost. On the other end, we expect that further improving the drone's ability to safely interact with vegetation will reduce the sampling effort. For example, sliding the collector along a branch can increase the sampling surface area and collect more eDNA. Although this study was limited to sampling the outermost branches, access to the inner regions of the canopy will allow the drone to reach additional sampling points. This is a challenging task because the drone has to fly between very dense obstacles, potentially making its way through branches and leaves. Safely flying and traversing dense vegetation remains an open research challenge and will require the synergetic development of electronic skins (*57*) to detect the multiple contacts and collisions that can potentially occur anywhere on the drone, and robust control strategies to handle push and sliding on compliant structures. Faster collection can instead be achieved with a fleet of eDrones (a multi-agent system) that can simultaneously sample a larger area (*58*).

Our results pave the way for a generation of robotic biodiversity explorers able to survey eDNA at different spatial and temporal scales. By allowing these robots to dwell in the environment, this biomonitoring paradigm would provide information on global biodiversity and potentially automate our ability to measure, understand and predict how the biosphere responds to human activity and environmental changes (*59*).

MATERIALS AND METHODS

Drone architecture

The eDrone uses a quadcopter layout consisting of a carbon-fiber frame, four brushless motors (Dys THOR 2408 - 2200KV) with 6-inch propellers (Gemfan 6040) controlled by an electronic speed controller (Hobbywing XRotor 40A 4in1 ESC). A flight controller (FC) stabilizes the attitude of the drone (BrainFPV, Radix LI). An Intel RealSense T261 tracking camera provides visual inertial estimation, and a Khadas VIM3 companion computer provides high-level position

controller, wireless communication, and additional on-board computations. The external force applied by the branch on the drone is measured by a Medusa F/T sensor (Bota Systems AG, Switzerland).

Cage manufacturing

The main links of the cage, the horizontal ring, and the vertical arcs are laser-cut (Trotec Speedy 360) from 3 mm medium-density fibreboard (MDF) panels. The components are connected via 3D printed elements (Stratasys F120) and fixed with screws. The collection flaps are made of fiberglass (FR-40-HF, 0.2 mm) and connected to the cage with screws. The cage is designed such that four collection flaps can be exposed simultaneously for sampling. The outer circular ring added for shielding the propellers is made of fiberglass as well. The cantilevers are made with 2-mm carbon beams and the high-friction material is DYCEM non-slip.

Control architecture

The complete sensing and control architecture of the eDrone is depicted in Fig. 8. The load cell measures the external force in the body frame, hence the HWR converts it into the world frame by using the orientation of the body frame with respect to the world frame, resulting into the global external force $\boldsymbol{F}_{ext}$. The attitude controller runs on the Flight Controller, and it takes as input the collective thrust and the reference orientation, which are sent by the position controller. We implement the position controller developed in (*60*), which can receive position and yaw reference. During the Descending and Leaning phases, the HWR sends vertical reference waypoints $\boldsymbol{p}_{ref} = \left[x, y, z - \Delta z\right]^T$, while during the resting phase it exploits the information about the amplitude and the direction of the force by commanding a 3D waypoint (as previously highlighted in Fig. 3C), following the equation:

$$\boldsymbol{p}_{resting} = \boldsymbol{p}_{ref} = \boldsymbol{p} - C_{gain} \frac{\boldsymbol{F}_{ext}}{\left\|\boldsymbol{F}_{ext}\right\|} \tag{1}$$

where C_{gain} is the controller gain that can be tuned depending on the force we want to apply on the branch.

Statistical analysis

To obtain the distributions of data that we used for the statistical analysis of performance for varying stiffness and misalignment between the drone and the perch below (see chapter Results), we extracted a single value of standard deviation of position error and mean of interaction force considering the interval of time of the resting phase, for each landing test. Therefore, upon N tests we had a distribution composed of N values. The Mann-Whitney U-test has been performed in MATLAB R2020a (MathWorks, MA, USA).

eDNA collection materials

Due to the difficulty of sampling eDNA from trees, there are limited references in literature about suitable materials for retrieving DNA traces from the bark of the branches (*27*). Inspired by the peeling technique exploited in forensic investigations, we used sterile adhesive tape, as it can be easily pressed against surfaces and retrieve particles containing eDNA. We selected Sellotape® (UK) based on (*61*), where they identified the efficiency of tape-lifting for the collection of cellular material. As a second collector material, we combined the adhesive properties of liquid sugar with cotton-based materials. Water facilitates the transfer of eDNA from dry substrates (*62*), while the sugar adds an adhesive action to the collector. We selected sterilized elastic cotton gauze (DermaPlast® Stretch, Hartmann) and humidified it with a natural, adhesive solution composed of a mixture of physiological serum (Triofan physiologic, Verfora®) and

DNAse/RNAse-free D(+)-Saccarose (CarlRoth®), 5 ml and 10 g respectively, stirred and stored in 10ml sterile tubes.

eDNA analysis

DNA extraction was performed following a modified protocol from (*32*) in a dedicated eDNA laboratory, equipped with positive air pressure, UV treatment, and frequent air renewal. Decontamination procedures were conducted before and after all manipulations. The samples were analyzed using a metazoan universal primer. When choosing a metabarcoding marker, there is always a trade-off between primer universality and taxonomic resolution of the amplified fragment (*63*). In this proof of concept, we used a very universal primer pair that amplifies all metazoa species since we had no clear expectations of which animal was leaving most of the DNA traces on the top of the branches. However, when using such universal markers, it is possible to detect a broad range of taxonomic groups, but sequence variation does not allow identification at species level, as reflected in the results of the analysis (Fig. 7). The amplification was carried out with 12 replicate PCRs per sample using 16S_Metazoa primers (16s_Metazoa_fwd AGTTACYYTAGGGATAACAGCG; 16s_Metazoa_rev CCGGTCTGAACTCAGATCAYGT) (*64*). The primers were 5'-labeled with an eight-nucleotide tag unique to each sample (with at least three differences between any pair of tags), allowing the assignment of each sequence to the corresponding sample during sequence analysis. The purified PCR products were pooled before the sequencing steps in equal volumes to achieve a theoretical sequencing depth of 100,000 reads per sample. PCR amplification and purification were performed in a room dedicated to amplified DNA analysis with negative air pressure and physically separated from the eDNA extraction room. Library preparation and sequencing on Illumina MiSeq sequencer were performed at DNAGensee (Le Bourget du Lac, France). The sequence reads were analyzed using programs implemented in the OBITools package (http://metabarcoding.org/obitools) (*65*) following the protocol described in (*66*). Detailed protocols of DNA extraction, amplification and sequencing, and bioinformatic analysis can be found in the Supplementary Materials.

Supplementary Materials

Text

Fig. S1. Constraint on the maximum admissible bending of the perch.

Fig. S2. Moment of force *M* acting on the drone's center of mass while resting on a flexible beam, as a function of the radius of the cage.

Fig. S3. Effect of non-zero initial deflection angle of the perch on the static equilibrium analysis.

Fig. S4. Comparison of the power consumption between the physical interaction, for different stiffnesses of the perch, and the hovering condition.

Fig. S5. Gazebo physical simulation of the landing strategy on a flexible cylindrical beam.

Table S1. Computation of the contact surface area.

Table S2. Computation of the stiffness of the perches.

Movie S1. Indoor landing experiments over perches with stiffness (K).

References and Notes

1. IPBES, Global assessment report on biodiversity and ecosystem services of the Intergovernmental Science-Policy Platform on Biodiversity and Ecosystem Services. (2019). doi: 10.5281/ZENODO.6417333.
2. M. Loreau, S. Naeem, P. Inchausti, J. Bengtsson, J. P. Grime, A. Hector, D. U. Hooper, M. A. Huston, D. Raffaelli, B. Schmid, D. Tilman, and D. A. Wardle, Biodiversity and ecosystem functioning: Current knowledge and future challenges. *Science (80-.).* **294**, 804–808, (2001). doi: 10.1126/science.1064088.
3. B. J. Cardinale, J. E. Duffy, A. Gonzalez, D. U. Hooper, C. Perrings, P. Venail, A. Narwani, G. M. MacE, D. Tilman, D. A. Wardle, A. P. Kinzig, G. C. Daily, M. Loreau, J. B. Grace, A. Larigauderie, D. S. Srivastava, and S. Naeem, Biodiversity loss and its impact on humanity. *Nature* **486**, 59–67, (2012). doi: 10.1038/nature11148.
4. D. U. Hooper, E. C. Adair, B. J. Cardinale, J. E. K. Byrnes, B. A. Hungate, K. L. Matulich, A. Gonzalez, J. E. Duffy, L. Gamfeldt, and M. I. O'Connor, A global synthesis reveals biodiversity loss as a major driver of ecosystem change. *Nat. 2012 4867401* **486**, 105–108, (2012). doi: 10.1038/nature11118.
5. M. Blicharska, R. J. Smithers, G. Mikusiński, P. Rönnbäck, P. A. Harrison, M. Nilsson, and W. J. Sutherland, Biodiversity's contributions to sustainable development. *Nat. Sustain.* **2**, 1083–1093, (2019). doi: 10.1038/s41893-019-0417-9.
6. H. Xu, Y. Cao, D. Yu, M. Cao, Y. He, M. Gill, and H. M. Pereira, Ensuring effective implementation of the post-2020 global biodiversity targets. *Nat. Ecol. Evol.* **5**, 411–418, (2021). doi: 10.1038/s41559-020-01375-y.
7. N. G. Yoccoz, J. D. Nichols, and T. Boulinier, Monitoring of biological diversity in space and time. *Trends Ecol. Evol.* **16**, 446–453, (2001). doi: 10.1016/S0169-5347(01)02205-4.
8. W. Turner, Conservation. Sensing biodiversity. *Science (80-.).* **346**, 301–302, (2014). doi: 10.1126/SCIENCE.1256014.
9. D. Leclère, M. Obersteiner, M. Barrett, S. H. M. Butchart, A. Chaudhary, A. De Palma, F. A. J. DeClerck, M. Di Marco, J. C. Doelman, M. Dürauer, R. Freeman, M. Harfoot, T. Hasegawa, S. Hellweg, J. P. Hilbers, S. L. L. Hill, F. Humpenöder, N. Jennings, T. Krisztin, *et al.*, Bending the curve of terrestrial biodiversity needs an integrated strategy. *Nature* **585**, 551–556, (2020). doi: 10.1038/s41586-020-2705-y.
10. J.-B. Mihoub, K. Henle, N. Titeux, L. Brotons, N. A. Brummitt, and D. S. Schmeller, Setting temporal baselines for biodiversity: the limits of available monitoring data for capturing the full impact of anthropogenic pressures. *Sci. Reports 2017 71* **7**, 1–13, (2017). doi: 10.1038/srep41591.
11. C. A. Soto-Navarro, M. Harfoot, S. L. L. Hill, J. Campbell, F. Mora, C. Campos, C. Pretorius, U. Pascual, V. Kapos, H. Allison, and N. D. Burgess, Towards a multidimensional biodiversity index for national application. *Nat. Sustain.* **4**, 933–942, (2021). doi: 10.1038/s41893-021-00753-z.
12. P. F. Thomsen and E. Willerslev, Environmental DNA - An emerging tool in conservation for monitoring past and present biodiversity. *Biol. Conserv.* **183**, 4–18, (2015). doi: 10.1016/j.biocon.2014.11.019.
13. K. Deiner, H. M. Bik, E. Mächler, M. Seymour, A. Lacoursière-Roussel, F. Altermatt, S. Creer, I. Bista, D. M. Lodge, N. Vere, M. E. Pfrender, and L. Bernatchez, Environmental DNA metabarcoding: Transforming how we survey animal and plant communities. *Mol. Ecol.* **26**, 5872–5895, (2017). doi: 10.1111/mec.14350.
14. I. B. Schnell, K. Bohmann, S. E. Schultze, S. R. Richter, D. C. Murray, M.-H. S. Sinding, D. Bass, J. E. Cadle, M. J. Campbell, R. Dolch, D. P. Edwards, T. N. E. Gray, T. Hansen, A. N. Q. Hoa, C. L. Noer, S. Heise-Pavlov, A. F. Sander Pedersen, J. C. Ramamonjisoa, M. E. Siddall, *et al.*, Debugging diversity - a pan-continental exploration of the potential of

terrestrial blood-feeding leeches as a vertebrate monitoring tool. *Mol. Ecol. Resour.* **18**, 1282–1298, (2018). doi: 10.1111/1755-0998.12912.
15. K. C. Beng and R. T. Corlett, Applications of environmental DNA (eDNA) in ecology and conservation: opportunities, challenges and prospects. *Biodivers. Conserv.* **29**, 2089–2121, (2020). doi: 10.1007/s10531-020-01980-0.
16. F. Roger, H. R. Ghanavi, N. Danielsson, N. Wahlberg, J. Löndahl, L. B. Pettersson, G. K. S. Andersson, N. Boke Olén, and Y. Clough, Airborne environmental DNA metabarcoding for the monitoring of terrestrial insects—A proof of concept from the field. *Environ. DNA* **00**, (2022). doi: https://doi.org/10.1002/edn3.290.
17. C. Lynggaard, M. F. Bertelsen, C. V. Jensen, M. S. Johnson, T. G. Frøslev, M. T. Olsen, and K. Bohmann, Airborne environmental DNA for terrestrial vertebrate community monitoring. *Curr. Biol.* **32**, 701-707.e5, (2022). doi: 10.1016/J.CUB.2021.12.014.
18. P. Taberlet, E. Coissac, M. Hajibabaei, and L. H. Rieseberg, Environmental DNA. *Mol. Ecol.* **21**, 1789–1793, (2012). doi: 10.1111/J.1365-294X.2012.05542.X.
19. A. Lyet, L. Pellissier, A. Valentini, T. Dejean, A. Hehmeyer, and R. Naidoo, eDNA sampled from stream networks correlates with camera trap detection rates of terrestrial mammals. *Sci. Reports 2021 111* **11**, 1–14, (2021). doi: 10.1038/s41598-021-90598-5.
20. N. K. Truelove, N. V. Patin, M. Min, K. J. Pitz, C. M. Preston, K. M. Yamahara, Y. Zhang, B. Y. Raanan, B. Kieft, B. Hobson, L. R. Thompson, K. D. Goodwin, and F. P. Chavez, Expanding the temporal and spatial scales of environmental DNA research with autonomous sampling. *Environ. DNA* **00**, 1–13, (2022). doi: 10.1002/EDN3.299.
21. L. F. Gonzalez, G. A. Montes, E. Puig, S. Johnson, K. Mengersen, and K. J. Gaston, Unmanned Aerial Vehicles (UAVs) and Artificial Intelligence Revolutionizing Wildlife Monitoring and Conservation. *Sensors* **16**, (2016). doi: 10.3390/s16010097.
22. O. M. Cliff, D. L. Saunders, and R. Fitch, Robotic ecology: Tracking small dynamic animals with an autonomous aerial vehicle. *Sci. Robot.* **3**, (2018). doi: 10.1126/SCIROBOTICS.AAT8409/SUPPL_FILE/AAT8409_SM.PDF.
23. J. C. Hodgson, R. Mott, S. M. Baylis, T. T. Pham, S. Wotherspoon, A. D. Kilpatrick, R. Raja Segaran, I. Reid, A. Terauds, and L. P. Koh, Drones count wildlife more accurately and precisely than humans. *Methods Ecol. Evol.* **9**, 1160–1167, (2018). doi: 10.1111/2041-210X.12974.
24. S. Kunal, B. Grant, S. Annie, and S. Mac, Multidrone aerial surveys of penguin colonies in Antarctica. *Sci. Robot.* **5**, eabc3000, (2020). doi: 10.1126/scirobotics.abc3000.
25. R. V Nichols, J. P. G. M. Cromsigt, and G. Spong, DNA left on browsed twigs uncovers bite-scale resource use patterns in European ungulates. *Oecologia* **178**, 275–284, (2015). doi: 10.1007/s00442-014-3196-z.
26. P. F. Thomsen and E. E. Sigsgaard, Environmental DNA metabarcoding of wild flowers reveals diverse communities of terrestrial arthropods. *Ecol. Evol.* **9**, 1665–1679, (2019). doi: 10.1002/ece3.4809.
27. R. E. Valentin, D. M. Fonseca, S. Gable, K. E. Kyle, G. C. Hamilton, A. L. Nielsen, and J. L. Lockwood, Moving eDNA surveys onto land: Strategies for active eDNA aggregation to detect invasive forest insects. *Mol. Ecol. Resour.* **20**, 746–755, (2020). doi: https://doi.org/10.1111/1755-0998.13151.
28. C. H. Cannon, C. Borchetta, D. L. Anderson, G. Arellano, M. Barker, G. Charron, J. M. LaMontagne, J. H. Richards, E. Abercrombie, L. F. Banin, X. Tagle Casapia, X. Chen, P. Degtjarenko, J. E. Dell, D. Durden, J. E. Guevara Andino, R. Hernández-Gutiérrez, A. D. Hirons, C. S. Kua, *et al.*, Extending Our Scientific Reach in Arboreal Ecosystems for Research and Management. *Front. For. Glob. Chang.* **4**, 712165, (2021). doi: 10.3389/FFGC.2021.712165.
29. A. Nakamura, R. L. Kitching, M. Cao, T. J. Creedy, T. M. Fayle, M. Freiberg, C. N.

Hewitt, T. Itioka, L. P. Koh, K. Ma, Y. Malhi, A. Mitchell, V. Novotny, C. M. P. Ozanne, L. Song, H. Wang, and L. A. Ashton, Forests and Their Canopies: Achievements and Horizons in Canopy Science. *Trends Ecol. Evol.* **32**, 438–451, (2017). doi: 10.1016/j.tree.2017.02.020.

30. J.-P. Ore, S. Elbaum, A. Burgin, B. Zhao, and C. Detweiler, Autonomous Aerial Water Sampling. *F. Serv. Robot.* 137–151, (2015). doi: 10.1007/978-3-319-07488-7_10.
31. H. Doi, Y. Akamatsu, Y. Watanabe, M. Goto, R. Inui, I. Katano, M. Nagano, T. Takahara, and T. Minamoto, Water sampling for environmental DNA surveys by using an unmanned aerial vehicle. *Limnol. Oceanogr. Methods* **15**, 939–944, (2017). doi: https://doi.org/10.1002/lom3.10214.
32. D. Pont, M. Rocle, A. Valentini, R. Civade, P. Jean, A. Maire, N. Roset, M. Schabuss, H. Zornig, and T. Dejean, Environmental DNA reveals quantitative patterns of fish biodiversity in large rivers despite its downstream transportation. *Sci. Reports 2018 81* **8**, 1–13, (2018). doi: 10.1038/s41598-018-28424-8.
33. F. Ruggiero, V. Lippiello, and A. Ollero, Aerial Manipulation: A Literature Review. *IEEE Robot. Autom. Lett.* **3**, 1957–1964, (2018). doi: 10.1109/LRA.2018.2808541.
34. G. Nava, Q. Sablé, M. Tognon, D. Pucci, and A. Franchi, Direct Force Feedback Control and Online Multi-Task Optimization for Aerial Manipulators. *IEEE Robot. Autom. Lett.* **5**, 331–338, (2020). doi: 10.1109/LRA.2019.2958473.
35. L. Peric, M. Brunner, K. Bodie, M. Tognon, and R. Siegwart, Direct Force and Pose NMPC with Multiple Interaction Modes for Aerial Push-and-Slide Operations. *IEEE Int. Conf. Robot. Autom.* 1801, (2021). doi: 10.3929/ETHZ-B-000476947.
36. T. Tomić, C. Ott, and S. Haddadin, External wrench estimation, collision detection, and reflex reaction for flying robots. *IEEE Trans. Robot.* **33**, 1467–1482, (2017). doi: 10.1109/TRO.2017.2750703.
37. R. Rashad, J. B. C. Engelen, and S. Stramigioli, Energy tank-based wrench/impedance control of a fully-actuated hexarotor: A geometric port-hamiltonian approach. *Proc. - IEEE Int. Conf. Robot. Autom.* 6418–6424, (2019). doi: 10.1109/ICRA.2019.8793939.
38. F. Augugliaro and R. D'Andrea, Admittance control for physical human-quadrocopter interaction. *2013 Eur. Control Conf. ECC 2013* 1805–1810, (2013). doi: 10.23919/ecc.2013.6669643.
39. A. Y. Mersha, S. Stramigioli, and R. Carloni, Variable impedance control for aerial interaction. *IEEE Int. Conf. Intell. Robot. Syst.* 3435–3440, (2014). doi: 10.1109/IROS.2014.6943041.
40. B. Yüksel, C. Secchi, H. H. Bülthoff, and A. Franchi, Aerial physical interaction via IDA-PBC. *Int. J. Rob. Res.* **38**, 403–421, (2019). doi: 10.1177/0278364919835605.
41. K. Hang, X. Lyu, H. Song, J. A. Stork, A. M. Dollar, D. Kragic, and F. Zhang, Perching and resting-A paradigm for UAV maneuvering with modularized landing gears. *Sci. Robot.* **4**, (2019). doi: 10.1126/scirobotics.aau6637.
42. W. R. T. Roderick, M. R. Cutkosky, and D. Lentink, Bird-inspired dynamic grasping and perching in arboreal environments. *Sci. Robot.* **6**, 7562, (2021). doi: 10.1126/SCIROBOTICS.ABJ7562.
43. A. Briod, P. Kornatowski, J.-C. Zufferey, and D. Floreano, A Collision-resilient Flying Robot. *J. F. Robot.* **31**, 496–509, (2014). doi: 10.1002/rob.21495.
44. P. Sareh, P. Chermprayong, M. Emmanuelli, H. Nadeem, and M. Kovac, Rotorigami: A rotary origami protective system for robotic rotorcraft. *Sci. Robot.* **3**, 5228, (2018). doi: 10.1126/scirobotics.aah5228.
45. K. Alexis, G. Darivianakis, M. Burri, and R. Siegwart, Aerial robotic contact-based inspection: planning and control. *Auton. Robots* **40**, 631–655, (2016). doi: 10.1007/s10514-015-9485-5.

46. A. E. Jimenez-Cano, P. J. Sanchez-Cuevas, P. Grau, A. Ollero, and G. Heredia, Contact-Based Bridge Inspection Multirotors: Design, Modeling, and Control Considering the Ceiling Effect. *IEEE Robot. Autom. Lett.* **4**, 3561–3568, (2019). doi: 10.1109/LRA.2019.2928206.
47. K. Bodie, M. Brunner, M. Pantic, S. Walser, P. Pfandler, U. Angst, R. Siegwart, and J. Nieto, Active Interaction Force Control for Contact-Based Inspection with a Fully Actuated Aerial Vehicle. *IEEE Trans. Robot.* **37**, 709–722, (2021). doi: 10.1109/TRO.2020.3036623.
48. M. Ryll, G. Muscio, F. Pierri, E. Cataldi, G. Antonelli, F. Caccavale, D. Bicego, and A. Franchi, 6D interaction control with aerial robots: The flying end-effector paradigm. *Int. J. Rob. Res.* **38**, 1045–1062, (2019). doi: 10.1177/0278364919856694.
49. A. Ollero, M. Tognon, A. Suarez, D. Lee, and A. Franchi, Past, Present, and Future of Aerial Robotic Manipulators. *IEEE Trans. Robot.* **38**, 626–645, (2021). doi: 10.1109/TRO.2021.3084395.
50. A. van Casteren, W. I. Sellers, S. K. S. Thorpe, S. Coward, R. H. Crompton, and A. R. Ennos, Factors Affecting the Compliance and Sway Properties of Tree Branches Used by the Sumatran Orangutan (Pongo abelii). *PLoS One* **8**, e67877, (2013). doi: 10.1371/JOURNAL.PONE.0067877.
51. S. K. S. Thorpe, R. H. Crompton, and R. M. Alexander, Orangutans use compliant branches to lower the energetic cost of locomotion. *Biol. Lett.* **3**, 253–256, (2007). doi: 10.1098/rsbl.2007.0049.
52. H. C. Astley, A. Haruta, and T. J. Roberts, Robust jumping performance and elastic energy recovery from compliant perches in tree frogs. *J. Exp. Biol.* **218**, 3360–3363, (2015). doi: 10.1242/jeb.121715.
53. N. Hunt, J. Judy, L. F. Jacobs, and R. J. Full, Acrobatic squirrels learn to leap and land on tree branches without falling. *Science (80-.).* **373**, 697–700, (2021). doi: 10.1126/science.abe5753.
54. K. E. Crandell, A. F. Smith, O. L. Crino, and B. W. Tobalske, Coping with compliance during take-off and landing in the diamond dove (Geopelia cuneata). *PLoS One* **13**, 1–14, (2018). doi: 10.1371/journal.pone.0199662.
55. R. E. Valentin, K. E. Kyle, M. C. Allen, D. J. Welbourne, and J. L. Lockwood, The state, transport, and fate of aboveground terrestrial arthropod eDNA. *Environ. DNA* **3**, 1081–1092, (2021). doi: 10.1002/EDN3.229.
56. T.-H. Macher, R. Schütz, T. Hörren, A. J. Beermann, and F. Leese, It's raining species: Rainwash eDNA metabarcoding as a minimally invasive method to assess tree canopy invertebrate diversity. *bioRxiv* 2022.03.24.485661, (2022). doi: 10.1101/2022.03.24.485661.
57. B. Shih, D. Shah, J. Li, T. G. Thuruthel, Y. L. Park, F. Iida, Z. Bao, R. Kramer-Bottiglio, and M. T. Tolley, Electronic skins and machine learning for intelligent soft robots. *Sci. Robot.* **5**, 9239, (2020). doi: 10.1126/SCIROBOTICS.AAZ9239/ASSET/FB86D6D2-9D34-4AC2-9F75-D62000F8F7EE/ASSETS/GRAPHIC/AAZ9239-F6.JPEG.
58. X. Zhou, X. Wen, Z. Wang, Y. Gao, H. Li, Q. Wang, T. Yang, H. Lu, Y. Cao, C. Xu, and F. Gao, Swarm of micro flying robots in the wild. *Sci. Robot.* **7**, (2022). doi: 10.1126/SCIROBOTICS.ABM5954/SUPPL_FILE/SCIROBOTICS.ABM5954_SOFTWARE.ZIP.
59. D. A. Bohan, C. Vacher, A. Tamaddoni-Nezhad, A. Raybould, A. J. Dumbrell, and G. Woodward, Next-Generation Global Biomonitoring: Large-scale, Automated Reconstruction of Ecological Networks. *Trends Ecol. Evol.* **32**, 477–487, (2017). doi: 10.1016/j.tree.2017.03.001.
60. M. Faessler, A. Franchi, and D. Scaramuzza, Differential Flatness of Quadrotor Dynamics

Subject to Rotor Drag for Accurate Tracking of High-Speed Trajectories. *IEEE Robot. Autom. Lett.* **3**, 620–626, (2018). doi: 10.1109/LRA.2017.2776353.
61. P. Kanokwongnuwut, K. Paul Kirkbride, and A. Linacre, An assessment of tape-lifts. *Forensic Sci. Int. Genet.* **47**, (2020). doi: 10.1016/J.FSIGEN.2020.102292/ATTACHMENT/DA991054-AA59-49E5-BEFE-1029EE304007/MMC5.DOCX.
62. R. van Oorschot, D. G. Phelan, S. Furlong, G. M. Scarfo, N. L. Holding, and M. J. Cummins, Are you collecting all the available DNA from touched objects? *Int. Congr. Ser.* **1239**, 803–807, (2003). doi: 10.1016/S0531-5131(02)00498-3.
63. T. Riaz, W. Shehzad, A. Viari, F. Pompanon, P. Taberlet, and E. Coissac, ecoPrimers: inference of new DNA barcode markers from whole genome sequence analysis. *Nucleic Acids Res.* **39**, e145, (2011). doi: 10.1093/NAR/GKR732.
64. R. P. Kelly, J. L. O'Donnell, N. C. Lowell, A. O. Shelton, J. F. Samhouri, S. M. Hennessey, B. E. Feist, and G. D. Williams, Genetic signatures of ecological diversity along an urbanization gradient. *PeerJ* **4**, 1–20, (2016). doi: 10.7717/PEERJ.2444/SUPP-3.
65. F. Boyer, C. Mercier, A. Bonin, Y. Le Bras, P. Taberlet, and E. Coissac, obitools: a unix-inspired software package for DNA metabarcoding. *Mol. Ecol. Resour.* **16**, 176–182, (2016). doi: 10.1111/1755-0998.12428.
66. A. Valentini, P. Taberlet, C. Miaud, R. Civade, J. Herder, P. F. Thomsen, E. Bellemain, A. Besnard, E. Coissac, F. Boyer, C. Gaboriaud, P. Jean, N. Poulet, N. Roset, G. H. Copp, P. Geniez, D. Pont, C. Argillier, J. M. Baudoin, *et al.*, Next-generation monitoring of aquatic biodiversity using environmental DNA metabarcoding. *Mol. Ecol.* **25**, 929–942, (2016). doi: 10.1111/MEC.13428.
67. S. Kirchgeorg and S. Mintchev, HEDGEHOG: Drone Perching on Tree Branches with High-Friction Origami Spines. *IEEE Robot. Autom. Lett.* **7**, 602–609, (2021). doi: 10.1109/LRA.2021.3130378.
68. F. Furrer, M. Burri, M. Achtelik, and R. Siegwart, RotorS - A modular gazebo MAV simulator framework. *Stud. Comput. Intell*. in book *Robot operating system (ROS): the complete reference* **625**, 595–625, (2016), doi: 10.1007/978-3-319-26054-9_23/FIGURES/13.
69. Biggs, J., Ewald, N., Valentini, A., Gaboriaud, C., Dejean, T., Griffiths, R.A., Foster, J., Wilkinson, J.W., Arnell, A., Brotherton, P., Williams, P., Dunn, F. Using eDNA to develop a national citizen science-based monitoring programme for the great crested newt (Triturus cristatus). *Biol. Conserv.* **183**, 19–28, (2015). https://doi.org/10.1016/j.biocon.2014.11.029
70. Morgulis, A., Coulouris, G., Raytselis, Y., Madden, T.L., Agarwala, R., Schäffer, A.A. Database indexing for production MegaBLAST searches. *Bioinformatics* **24**, 1757–1764, (2008). https://doi.org/10.1093/bioinformatics/btn322
71. Zhang, Z., Schwartz, S., Wagner, L., Miller, W. A Greedy Algorithm for Aligning DNA Sequences. *J. Comput. Biology.* **7**, 203–214, (2000). https://doi.org/10.1089/10665270050081478
72. Schnell, I.B., Bohmann, K., Gilbert, M.T.P. Tag jumps illuminated – reducing sequence-to-sample misidentifications in metabarcoding studies. *Mol. Ecol. Resour.* **15**, 1289–1303, (2015). https://doi.org/10.1111/1755-0998.12402
73. Barba, D.M., Miquel, C., Boyer, F., Mercier, C., Rioux, D., Coissac, E., Taberlet, P. DNA metabarcoding multiplexing and validation of data accuracy for diet assessment: application to omnivorous diet. *Mol. Ecol. Resour.* **14**, 306-323, (2014). https://doi.org/10.1111/1755-0998.12188/full

74. Leonard, J.A., Shanks, O., Hofreiter, M., Kreuz, E., Hodges, L., Ream, W., Wayne, R.K., Fleischer, R.C. Animal DNA in PCR reagents plagues ancient DNA research. *J. Archaeol. Sci.* **34**, 1361–1366, (2007). https://doi.org/10.1016/j.jas.2006.10.023

Acknowledgments: We thank C. Geckeler and G. Pestalozzi for video recording and photography (respectively) during outdoor flight experiments. We thank E. Kaufmann for helping to debug the quadcopter during the initial assembly. We thank Marco Tognon who offered initial insights about the system stability. We thank M. Schlegel for offering suggestions regarding the collector materials. We thank SPYGEN staff for technical support in the eDNA laboratory.

Funding: This work was supported by the Swiss National Science Foundation through the research grant number 186865.

Author contributions: E.A., K.D., and S.M. conceived the project. E.A. and S.M. investigated the methodology and E.A. conducted numerical simulation of the static equilibrium. E.A. conceptualized and implemented the HWR, supported with physical simulations. E.A. and S.M. conceptualized the design of the eDrone. E.A. and S.K. developed the drone. E.A. conducted the indoor tests and performed the statistical data analysis. E.A. formalized and prepared the collector materials, and together with S.K. performed the outdoor experiments. A.V. supervised the eDNA analysis (extraction, amplification) and performed the bioinformatics analysis. L.P. and K.D. provided useful insights about the collection of eDNA from terrestrial ecosystems (general information and potential collector materials). E.A. and S.M. prepared the manuscript and all the authors provided feedback during subsequent revisions. S.M. administered the research, providing funding and principal supervision.

Competing interests: A.V. is co-founder and a research scientist in a private company specialized in the use of eDNA for biodiversity monitoring (SPYGEN). K.D. is co-founder and CEO of a private company that builds DNA-based biodiversity monitoring systems using environmental DNA (SimplexDNA AG).

Data and materials availability: All data are available in the main text or the supplementary materials. The Illumina raw sequence data are available online at 10.6084/m9.figshare.20141069. The HWR is available on github at https://github.com/erl-ethz/haptic_waypoint_replanner.

Figures

Movie 1. Collecting eDNA with the eDrone. The drone combines a haptic-based control strategy with a protective cage to land on tree branches. Surface eDNA is then collected using an adhesive surface integrated into the cage.

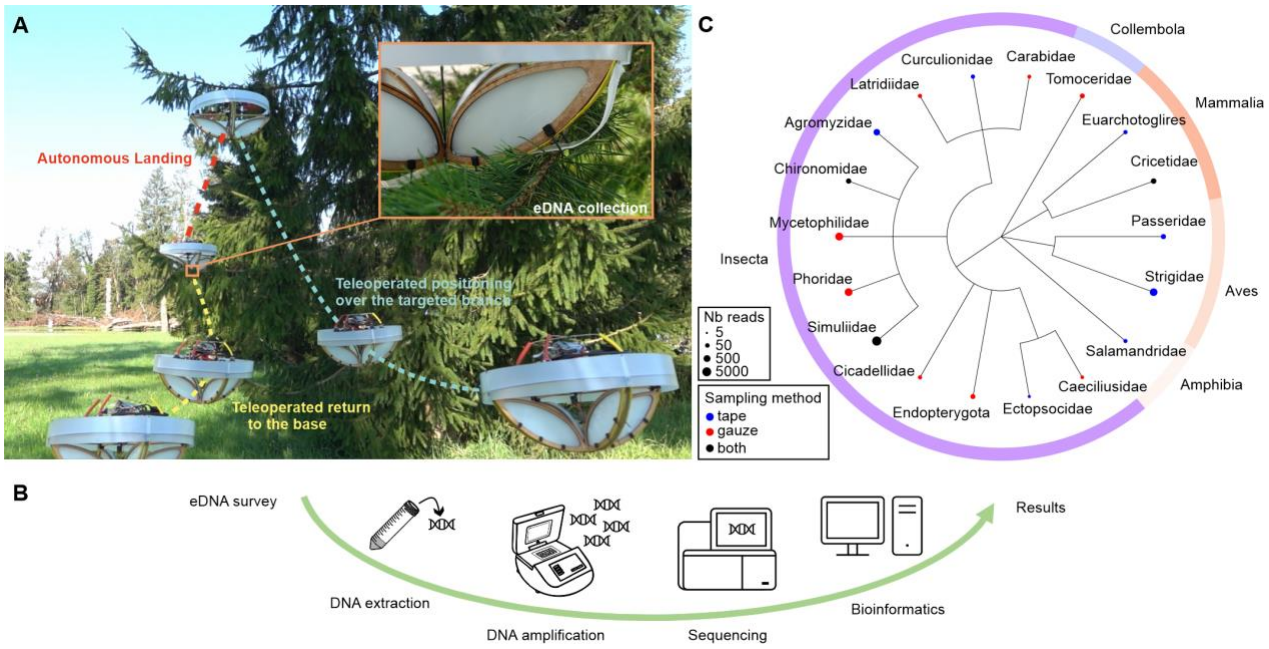

Fig. 1. Scheme of the biodiversity survey with an eDNA collection drone. (**A**) The eDrone is teleoperated above a targeted branch; it autonomously lands onto the branch and establishes a stable contact to collect the eDNA; after the sampling, the eDrone can be teleoperated back to the base station and the samples can be retrieved, preserved, and shipped to the eDNA laboratory. (**B**) The eDNA is extracted, amplified with universal primers, and sequenced. The results are generated by comparing environmental sampled sequences to a database for species identification. (**C**) Collected species (class and family) identified from the 14 samples collected with the eDrone in this proof-of-concept study. For each species, the number of DNA reads (Nb) and the sampling method that identified it are reported.

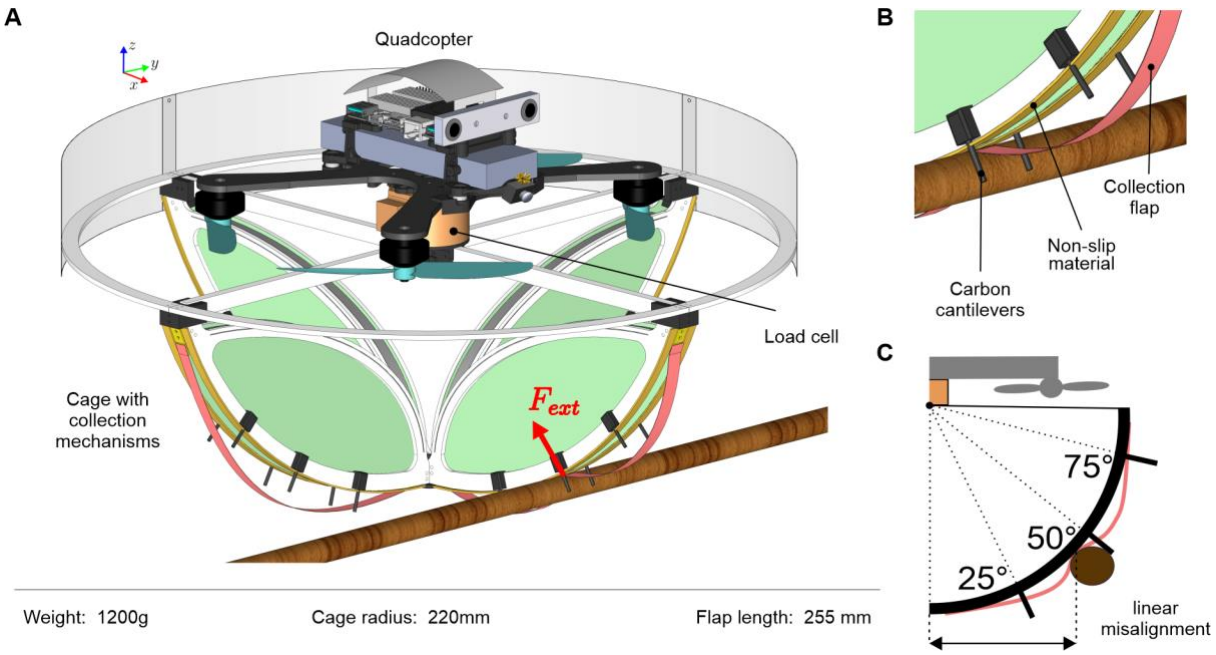

Fig. 2. eDrone architecture. (**A**) Perspective view of the eDrone 3D model with the main components. The external force (F_{ext}) applied by the branch is measured by a six-axis load cell that connects the cage with the frame of the drone. (**B**) Detailed view of the eDNA collection flap, non-slip material and carbon cantilevers added to improve grip on the bark. (**C**) Side view of the carbon cantilevers placed at 25°, 50°, and 75° on each unit of the hemisphere.

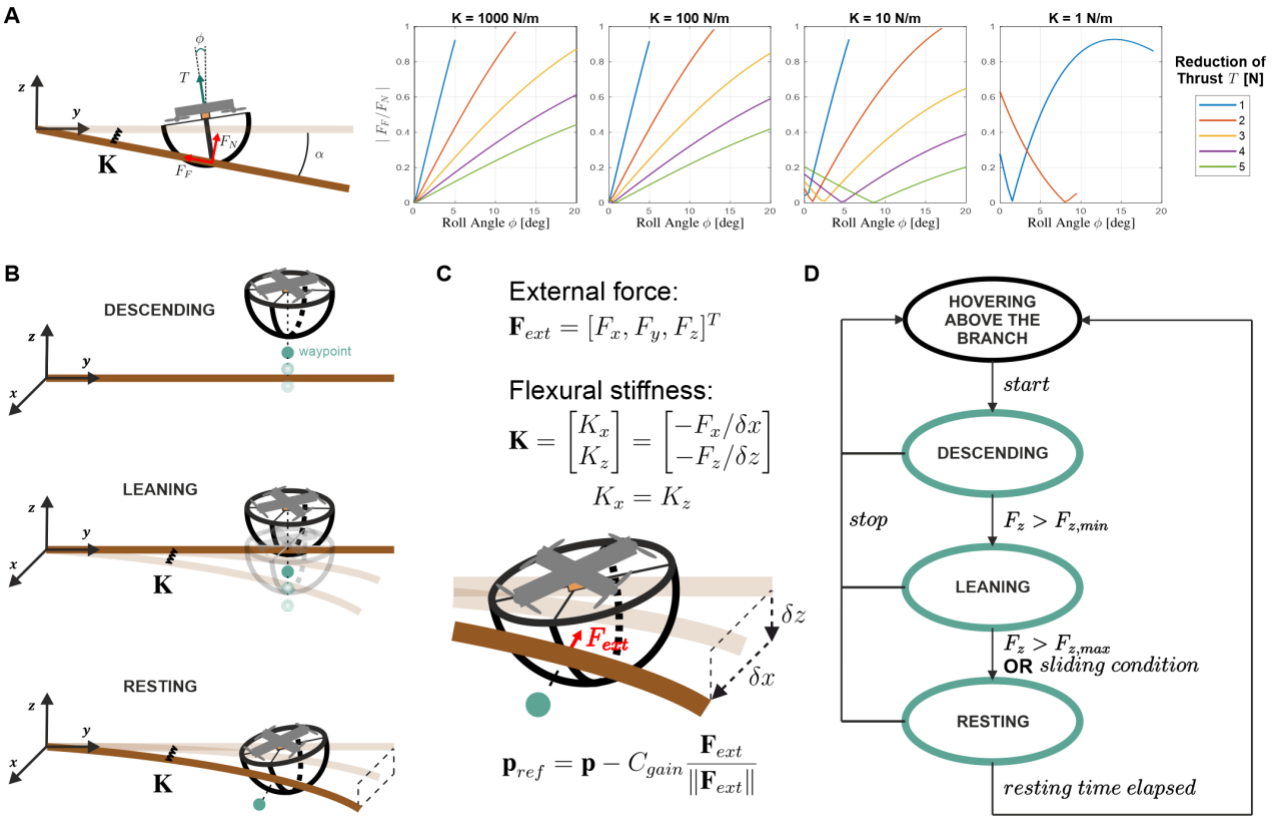

Fig. 3. Landing strategy. (**A**) Main result of the analysis of the static equilibrium of the drone on a hinged beam (2D case). Ratio between the friction and the normal force ($|F_F / F_N|$) as function of the drone tilt angle (ϕ). (**B**) Conceptual drawing of the three phases of the landing (Descending, Leaning, Resting). (**C**) The branch is assumed to behave as an elastic beam. The flexural stiffness of the perch is defined as the vector containing the stiffness value in the two directions of bending (the two values are assumed to be equal). The external force measured by the sensor, and transformed in the world frame, contains three components which are fully exploited during the resting phase to replan the waypoint and reduce the slippage. (**D**) State machine of the landing strategy.

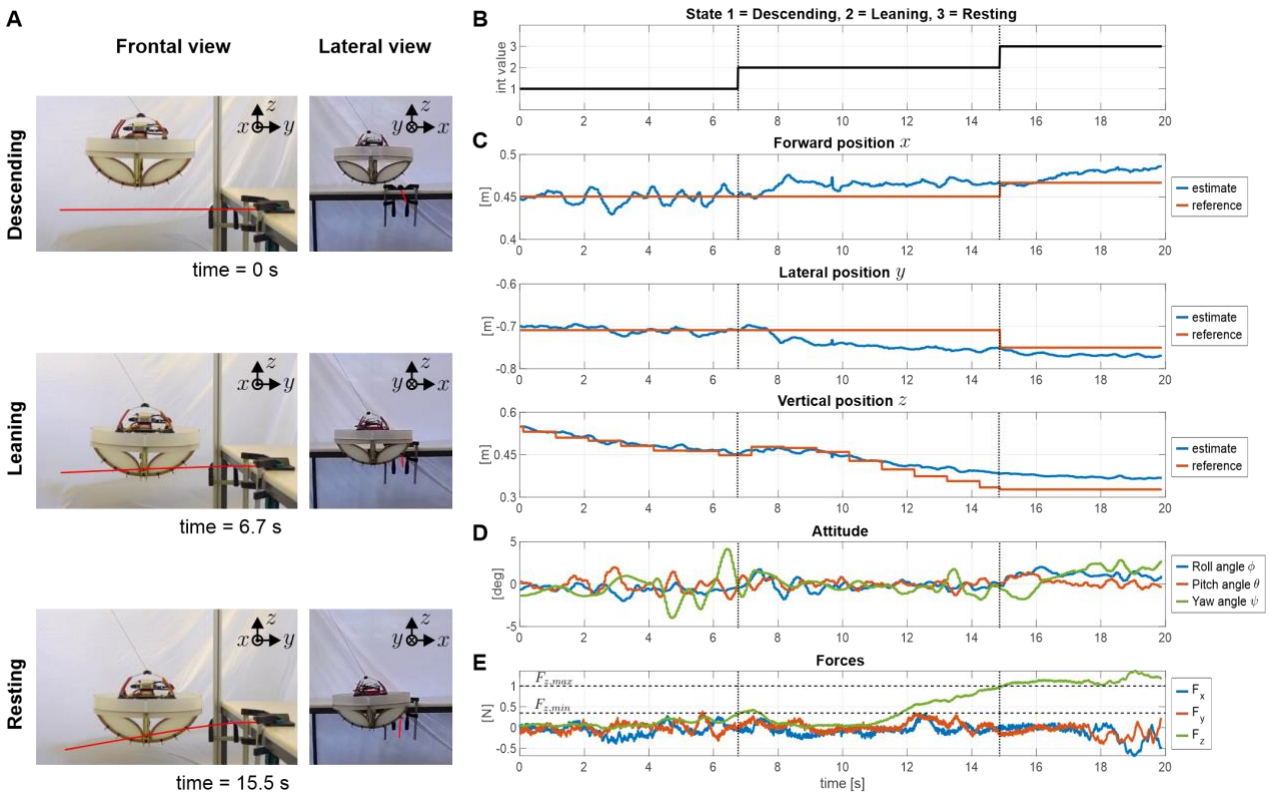

Fig. 4. Experiment of landing on a flexible beam (K = 1 N/m). (**A**) Still frames of the three phases of the strategy. Frontal and lateral view. (**B**) Phases of the state machine. Evolution of drone position (**C**), attitude (**D**), and interaction force (**E**) over time.

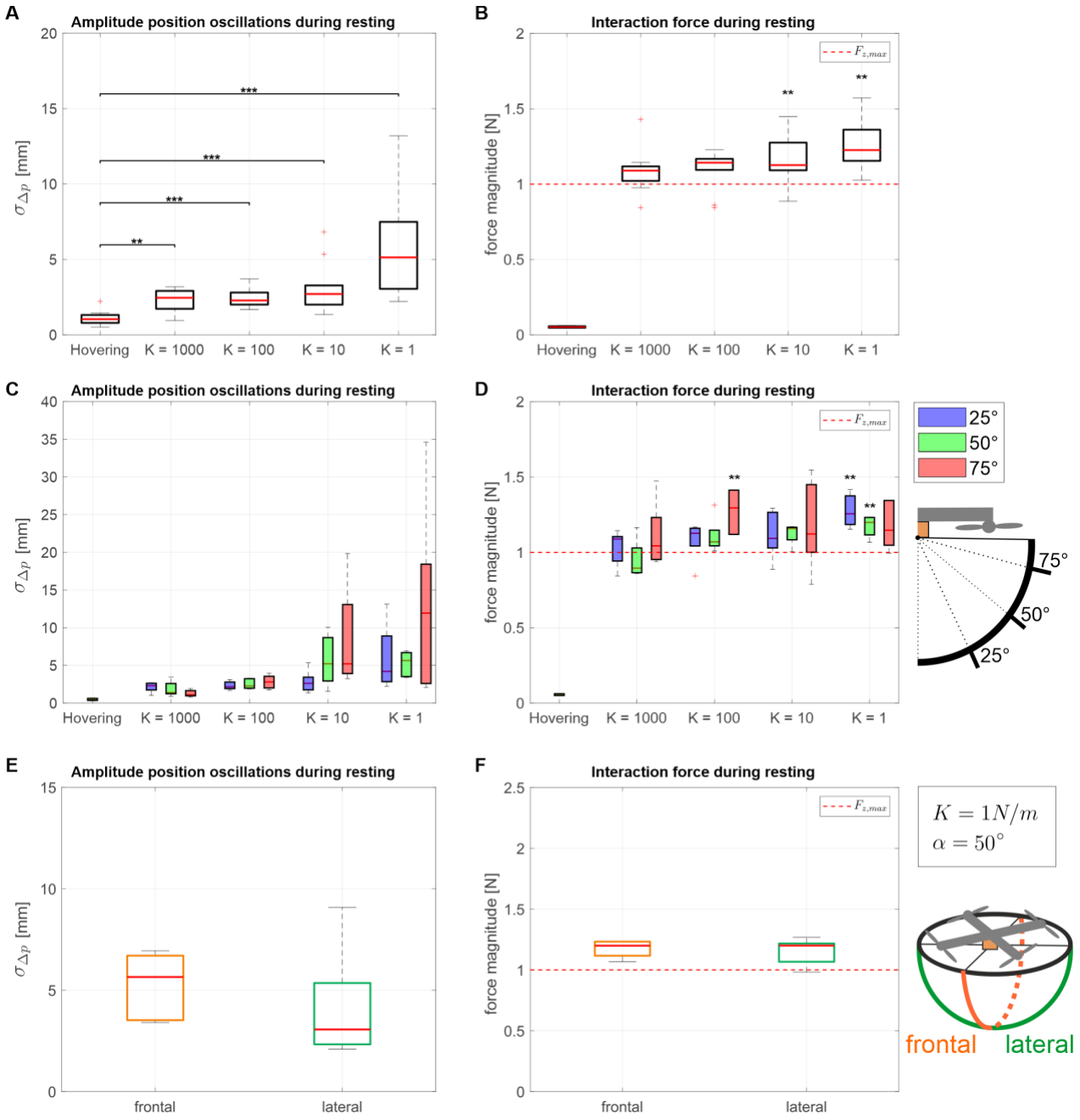

Fig. 5. Experimental validation of the interaction strategy. (**A**) Analysis of the performance during the resting phase with no misalignment: oscillations of the position from the mean value (Mann-Whitney U test; N = 10 for each stiffness; median and 25th and 75th percentiles; ** P < 0.01, *** P < 0.001). (**B**) Interaction force exchanged between the drone and the perch compared to the maximum force threshold (Mann-Whitney U test; N = 10 for each stiffness; median and 25th and 75th percentiles; ** P < 0.01). Total number of experiments over the range of stiffness = 40. (**C**) Robustness to linear misalignments in terms of position oscillations (Mann-Whitney U test; N = 5 for each stiffness and for each angle; ** P < 0.01 for all the boxplots compared to the hovering conditions, not added to the plot for clarity of the figure). (**D**) Robustness to linear misalignments in terms of interaction force (Mann-Whitney U test; N = 5 for each stiffness and for each angle; ** P < 0.01). Total number of experiments over the range of stiffness and angles = 60. (**E, F**) Robustness to angular misalignments (Mann-Whitney U test; N = 5 for each axis; median and 25th and 75th percentiles; P > 0.5). Total number of experiments = 10.

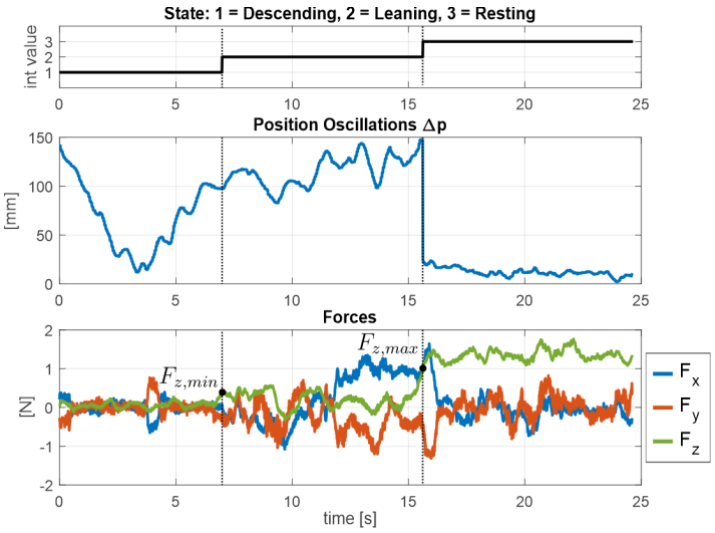

Fig. 6. Example of outdoor test. Position oscillations and the components of the external force (F_{ext}) landing on the pine tree branch shown in Fig. 1.

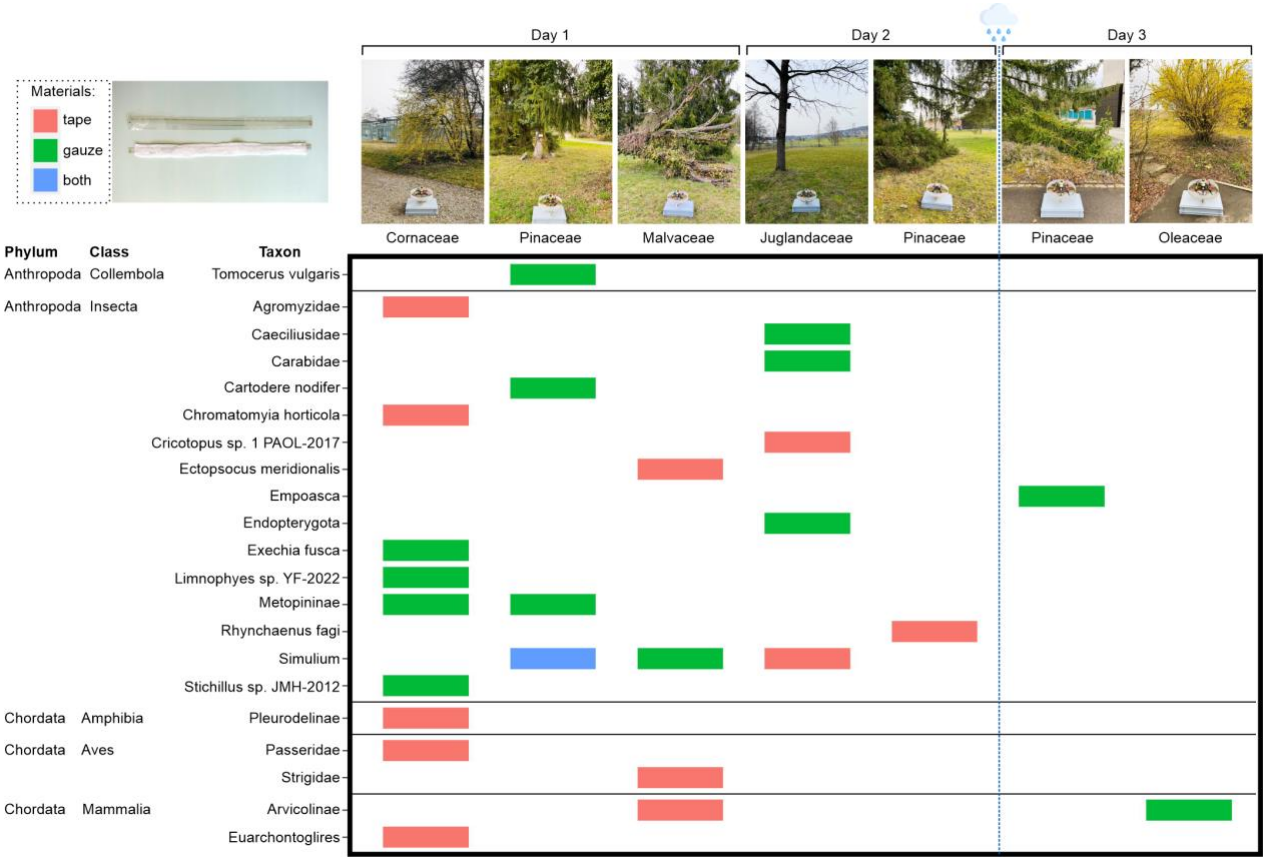

Fig. 7. eDNA sampling experiments reporting the detected species (phylum, class, and taxon) in relation with the specific collector materials and tree species. The analysis resulted in the identification of 21 taxa, spanning five animal classes: Insecta, Mammalia, Aves, Collembola, and Amphibia. Such a result validates that our eDrone collects eDNA by touching tree branches. The blue dashed line represents the rain occurred during the night between the second and the third day.

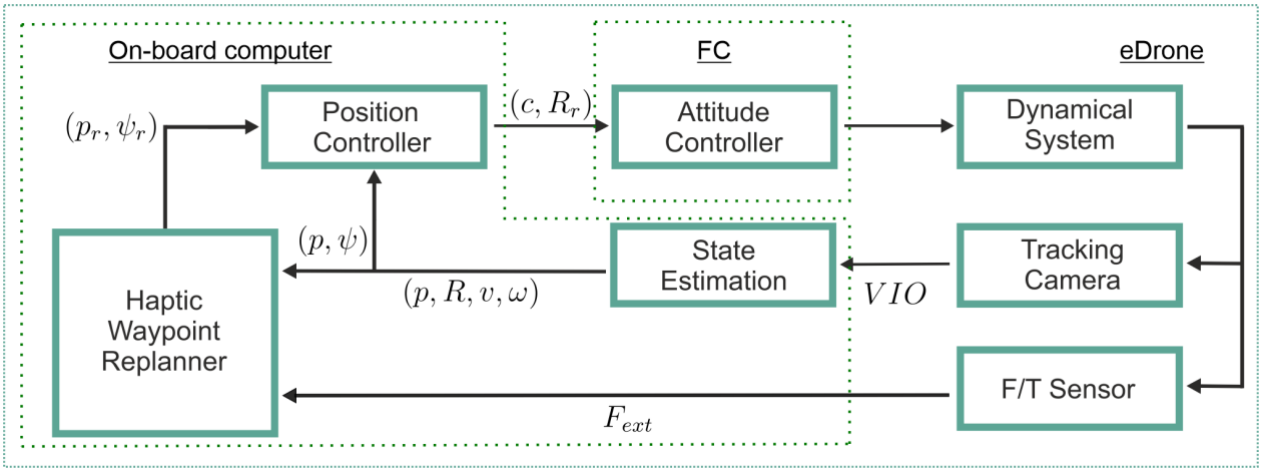

Fig. 8. Block diagram of the system components and the control architecture. The force sensor provides external forces information to the HWR (Haptic Waypoint Replanner). The state estimator provides instead position, orientation, linear and angular velocities (the robot's state). The position controller receives reference waypoints from the HWR as input and outputs collective thrust and reference orientation to the Flight Controller.